Early paper draft: Search for new particles decaying to dijets in pp collisions at $\sqrt{s} = 10$ TeV

Sertac Ozturk
Cukurova University

Robert Harris and Konstantinos Kousouris
Fermilab

Chiyoung Jeong and Sung-Won Lee
Texas Tech University

Abstract

1   We present an early paper draft, which contains only simulation and theory, but what

2   follows is written as if it were reporting a real measurement of early CMS data.

3

4   We have used 10 pb^{-1} of integrated luminosity from the CMS experiment at the Large

5   Hadron Collider at CERN to search for new particles decaying to dijets. The measured

6   dijet mass spectrum agrees with QCD predictions. We exclude at the 95% confidence level

7   models containing the following new particles: axigluons and flavor universal colorons with

8   mass below 1.8 TeV/c^2, excited quarks with mass below 1.9 TeV/c^2 and E_6 diquarks with

9   mass below 1.0 TeV/c^2 and within the range 1.3–1.8 TeV/c^2.

Within the standard model events with two energetic jets (dijets) are expected to arise in proton-proton collisions from parton-parton scattering. The outgoing scattered partons manifest themselves as hadronic jets. The dijet mass spectrum predicted by Quantum Chromodynamics (QCD) falls smoothly and steeply with increasing dijet mass. Many extensions of the standard model predict the existence of new massive objects that couple to quarks (q) and gluons (g), and result in resonant structures in the dijet mass spectrum. In this paper we report a search for narrow resonances in the dijet mass spectrum, measured with the Compact Muon Solenoid (CMS) detector at the CERN Large Hadron Collider, at a proton-proton collision energy of $\sqrt{s} = 10$ TeV.

In addition to this generic search, we specifically search for the following eight models of dijet resonances. First, in a model where the symmetry group $SU(3)$ of QCD is replaced by the chiral symmetry $SU(3)_L \times SU(3)_R$, there are axial vector particles called axigluons A which decay to $q\bar{q}$ [1]. Second, the flavor-universal coloron model also embeds the $SU(3)$ of QCD in a larger gauge group, and predicts the presence of a color-octet coloron C which decays to $q\bar{q}$ [2]. Third, if quarks are composite particles then excited states are expected, and we search for mass degenerate excited quarks q^* that decay to qg [3]. Fourth, grand unified theory based on the E_6 gauge group predicts the presence of scalar diquarks D and D^c which decays to $\bar{q}\bar{q}$ and qq [4]. Fifth, models of technicolor predict the presence of color octet technirhos ρ_T which decay to $q\bar{q}$ and gg [5]. Sixth, the Randall-Sundrum model of extra dimensions predicts massive gravitons G which decay to $q\bar{q}$ and gg [6]. Seventh and Eighth, models which propose new gauge symmetries often predict

2

31 new gauge bosons W' and Z' which decay to $q\bar{q}$ [7].

32 A detailed description of the CMS experiment can be found elsewhere [8, 9]. The

33 CMS coordinate system has the origin at the center of the detector, z-axis points along

34 the beam direction toward the west, with the transverse plane perpendicular to the beam.

35 We define ϕ to be the azimuthal angle, θ to be the polar angle and the pseudorapidity

36 as $\eta \equiv -\ln(\tan[\theta/2])$. The central feature of the CMS apparatus is a superconducting

37 solenoid, of 6 m internal diameter. Within the field volume are the silicon pixel and

38 strip tracker, and the barrel and endcap calorimeters ($|\eta| < 3$): a crystal electromagnetic

39 calorimeter (ECAL) and a brass-scintillator hadronic calorimeter (HCAL). Outside the

40 field volume, in the forward region, there is an iron-quartz fiber hadronic calorimeter

41 ($3 < |\eta| < 5$). The HCAL and ECAL cells are grouped into towers, projecting radially

42 outward from the origin, for triggering purposes and to facilitate the jet reconstruction. In

43 the region $|\eta| < 1.74$ these projective calorimeter towers have segmentation $\Delta\eta = \Delta\phi =$

44 0.087, and the η and ϕ width progressively increases at higher values of η. The energy

45 in the HCAL and ECAL within each projective tower is summed to find the calorimeter

46 tower energy. Towers with $|\eta| < 1.3$ contain only cells from the barrel calorimeters, towers

47 in the transition region $1.3 < |\eta| < 1.5$ contain a mixture of barrel and endcap cells, and

48 towers in the region $1.5 < |\eta| < 3.0$ contain only cells from the endcap calorimeters.

49 Jets are reconstructed using the seedless infrared safe cone algorithm with cone size

50 $R = \sqrt{(\Delta\eta)^2 + (\Delta\phi)^2} = 0.7$ [10]. Below we will discuss three types of jets: reconstructed,

51 corrected and generated. The reconstructed jet energy, E, is defined as the scalar sum of

3

52 the calorimeter tower energies inside the jet. The jet momentum, $\vec{p}$, is the corresponding

53 vector sum: $\vec{p} = \sum E_i \hat{u}_i$ with $\hat{u}_i$ being the unit vector pointing from the origin to the energy

54 deposition E_i inside the cone. The jet transverse momentum, p_T, is the component of $\vec{p}$ in

55 the transverse plane. The E and $\vec{p}$ of a reconstructed jet are then corrected for the non-

56 linear response of the calorimeter to a generated jet. Generated jets come from applying

57 the same jet algorithm to the Lorentz vectors of stable generated particles before detector

58 simulation. On average, the p_T of a corrected jet is equal to the p_T of the corresponding

59 generated jet. The corrections estimated from a GEANT [11] simulation of the CMS

60 detector increase the average jet p_T by roughly 50% (10%) for 70 GeV (3 TeV) jets in

61 the region $|\eta| < 1.3$. Further details on jet reconstruction and jet energy corrections can

62 be found elsewhere [12, 13]. The jet measurements presented here are within the region

63 $|\eta| < 1.3$, where the sensitivity to new physics is expected to be the highest, and where the

64 reconstructed jet response variations as a function of η are both moderate and smooth.

65 The dijet system is composed of the two jets with the highest p_T in an event (leading

66 jets), and the dijet mass is given by $m = \sqrt{(E_1 + E_2)^2 - (\vec{p}_1 + \vec{p}_2)^2}$. We require both

67 leading jets have pseudorapidity $|\eta| < 1.3$. The estimated dijet mass resolution varies

68 from 9% at a dijet mass of 0.7 TeV to 4.5% at 5 TeV. We use data from the 2009-2010

69 running period corresponding to an integrated luminosity of 10 pb^{-1}. The sample we

70 use for this search was collected by requiring at least one jet in the high level trigger

71 with $p_T > 110$ GeV/c. The trigger efficiency, measured from a sample acquired with a

72 prescaled trigger with a lower p_T threshold, was greater than 99% for dijet mass above

4

420 GeV/c^2. Backgrounds from cosmic rays, beam halo, and detector noise are expected to occasionally produce events with large or unbalanced energy depositions. They are removed by requiring $\not{E}_T / \sum E_T < 0.3$ and $\sum E_T < 10$ TeV, where $\not{E}_T$ ($\sum E_T$) is the magnitude of the vector (scalar) sum of the transverse energies measured by all calorimeter towers in the event. This cut is more than 99% efficient for both QCD jet events and the signals of new physics considered. In the high p_T region relevant for this search, jet reconstruction is fully efficient.

In Fig. 1 we present the inclusive dijet mass distribution for $p\bar{p} \rightarrow 2$ leading jets + X, where X can be anything including additional jets. We plot the differential cross section versus dijet mass in bins approximately equal to the dijet mass resolution. The systematic uncertainty on the cross section arises predominantly from a 10% uncertainty on the jet energy correction, but also includes a 10% uncertainty on the luminosity. The data is compared to a prediction from PYTHIA [14] which includes a simulation of the CMS detector and the jet energy corrections. The data is also compared with a full QCD prediction at next-to-lowest order [15] convoluted with the dijet mass resolution of the CMS detector for corrected jets. Both predictions use CTEQ6 parton distributions [16] and a renormalization scale $\mu = p_T$. The data agrees with both predictions within the systematic uncertainties of the measurement. To test the smoothness of our measurement as a function of dijet mass, we fit the data with the parameterization

$d\sigma/dm = P0(1 - m/\sqrt{s} + P3m^2/s)^{P1}/m^{P2}$ with the four parameters $P0$, $P1$, $P2$ and $P3$. In Figs 2 we show both the data and the background fit, which has a χ^2 of 23 for 32

degrees of freedom. In Figure 3 we show the fractional difference between the data and the background fit. The data is well fit by the smooth parameterization and shows no evidence of new particles.

To set limits on dijet resonances it is sufficient to use the resonance line shape for only one new particle type assuming each new particle's natural half-width ($\Gamma/2$) is small compared to the dijet mass resolution. In Figs. 2 and 3 we show the predicted line shape for excited quarks (q^*) using the PYTHIA Monte Carlo [14] and a CMS detector simulation. The mass resolution has a Gaussian core from jet energy resolution and a long tail towards low mass from QCD radiation. We have used the q^* mass resonance curves in Figs. 2 and 3 to model the shape of all new particles decaying to dijets. We perform a binned maximum likelihood fit of the data to both the background parameterization and the signal hypothesis. The method gave a Poisson likelihood as a function of the signal cross section. This was done independently at 29 different values of new particle mass from 0.7 to 3.5 TeV/c^2 in 0.1 TeV/c^2 steps resulting in 29 statistical likelihood distributions from which we found initial 95% confidence level upper limit on the cross section including only statistical undertainties. Systematic uncertainties on the cross section limits are dominated by a 10% uncertainty in the jet energy scale. Variations in jet response to quarks and gluons made the cross section limit dependent on whether we chose a $q\bar{q}$ or gg resonance instead of our default qg resonance, and these variations were included as a systematic. The cross section limit also depended on the choice of background parameterization and uncertainties in the simulation of the dijet mass resolution. We combined

these uncertainties in quadrature and convoluted each of the 29 Poisson likelihoods with the Gaussian systematic uncertainty and found the final 95% confidence level upper limits on the cross section presented in Table I.

In Fig. 4 we compare our measured upper limit on the cross section times branching ratio for a new particle decaying to dijets to the theoretical predictions. The predictions are lowest order calculations with CTEQ6L parton distributions [16] for dijets with $|\eta| <$ 1.3. We exclude at 95% C.L. new particles in mass regions for which the theory curve lies above our upper limit. For axigluons (or flavor universal colorons) we exclude the mass range $0.7 < M(A) < 1.8$ TeV/c^2, extending the previous exclusions [17] of $120 < M(A) < 1250$ GeV/c^2 obtained by the Tevatron. For excited quarks we exclude the mass range $0.7 < M(q*) < 1.9$ TeV/c^2, extending the previous exclusions [17] of $260 < M(q*) < 870$ GeV/c^2. For E_6 diquarks we exclude the mass range $0.7 < M(D) < 1.0$ and $1.3 < M(D) < 1.8$ TeV/c^2, extending the previous exclusions [17] of $290 < M(D) < 630$ GeV/c^2.

In conclusion, the measured dijet mass spectrum is a smoothly falling distribution which agrees with the predictions of the standard model. We see no significant evidence for new particle production and set limits on axigluons, flavor universal colorons, excited quarks, and E_6 diquarks.

University of Cyprus (Cyprus); Academy of Sciences and NICPB (Estonia); Academy of Finland, ME and HIP (Finland); CEA and CNRS/IN2P3 (France); BMBF and DESY (Germany); GSRT (Greece); NKTH (Hungary); DAE and DST (India); IPM (Iran); UCD (Ireland); INFN (Italy); KICOS (Korea); CINVESTAV, CONACYT and UASLP-FAI (Mexico); PAEC (Pakistan); SCSR (Poland); FCT (Portugal); JINR (Armenia, Belarus, Georgia, Ukraine, Uzbekistan); MST and MAE (Russia); MSEP (Serbia); OCT (Spain); ETHZ, PSI, University of Zurich (Switzerland); NSC (Taipei); TUBITAK and TAEK (Turkey); STFC (United Kingdom); DOE and NSF (USA).

References

[1] P. Frampton and S. Glashow, Phys. Lett. **B190**, 157 (1987).

[2] E. Simmons, Phys. Rev. D55, 1678 (1997).

[3] U. Baur, I. Hinchliffe & D. Zeppenfeld, Int. J. Mod. Phys **A2**, 1285 (1987).

[4] J. Hewett and T. Rizzo, Phys. Rep. **183**, 193 (1989) and references therein.

[5] K. Lane and S. Mrenna, Phys. Rev. D67,115011(2003).

[6] L. Randall and R. Sundrum, Phys.Rev.Lett.83, 3370 (1999).

[7] E. Eichten, I. Hinchliffe, Kenneth D. Lane, C. Quigg, Rev.Mod.Phys.56:579-707 (1984).

[8] R. Adolphi et al., CMS Collaboration, JINST 3:S08004 (2008).

[154] [9] CMS Collaboration, Physics TDR Volume I, CERN-LHCC-2006-001.

[155] [10] G. P. Salam and G. Soyez, JHEP 0705:086 (2007).

[156] [11] S. Agostinelli *et al.* (GEANT4 Collaboration), Nucl. Instrum. Meth. A**506**, 250
[157]   (2003).

[158] [12] CMS Collaboration, CMS Physics Analysis Summary JME-07-002 (2008). at
[159]   http://cms-physics.web.cern.ch/cms-physics/public/JME-07-002-pas.pdf .

[160] [13] CMS Collaboration, CMS Physics Analysis Summary JME-07-003 (2008). at
[161]   http://cms-physics.web.cern.ch/cms-physics/public/JME-07-003-pas.pdf .

[162] [14] T. Sjostrand, L. Lonnblad, S. Mrenna, hep-ph/0108264.

[163] [15] Z. Nagy, Phys. Rev. D68:094002, 2003.

[164] [16] J. Pumplin *et al.* (CTEQ Collaboration), JHEP **07**, 012 (2002).

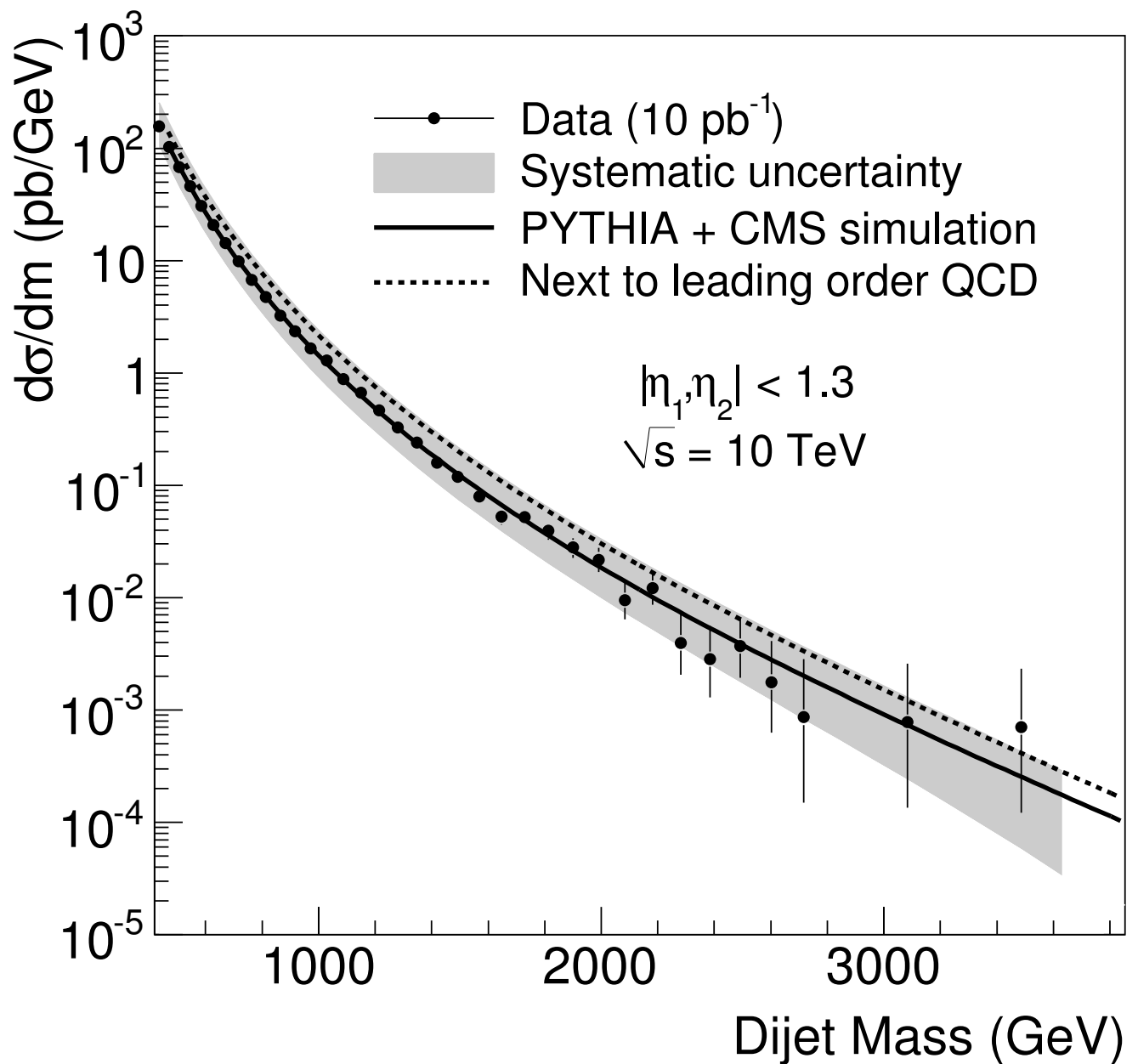[165] [17] T. Aaltonen et al., CDF Collaboration, arXiv:0812.4036, submitted to Phys. Rev. D.

Figure 1: The dijet mass distribution (points) compared to a simulation of QCD and the CMS detector (solid curve) and a next-to-leading order QCD calculation (dashed curve). The band shows the systematic uncertainties on the data. WARNING: CMS DATA IN THIS FIGURE IS FAKE
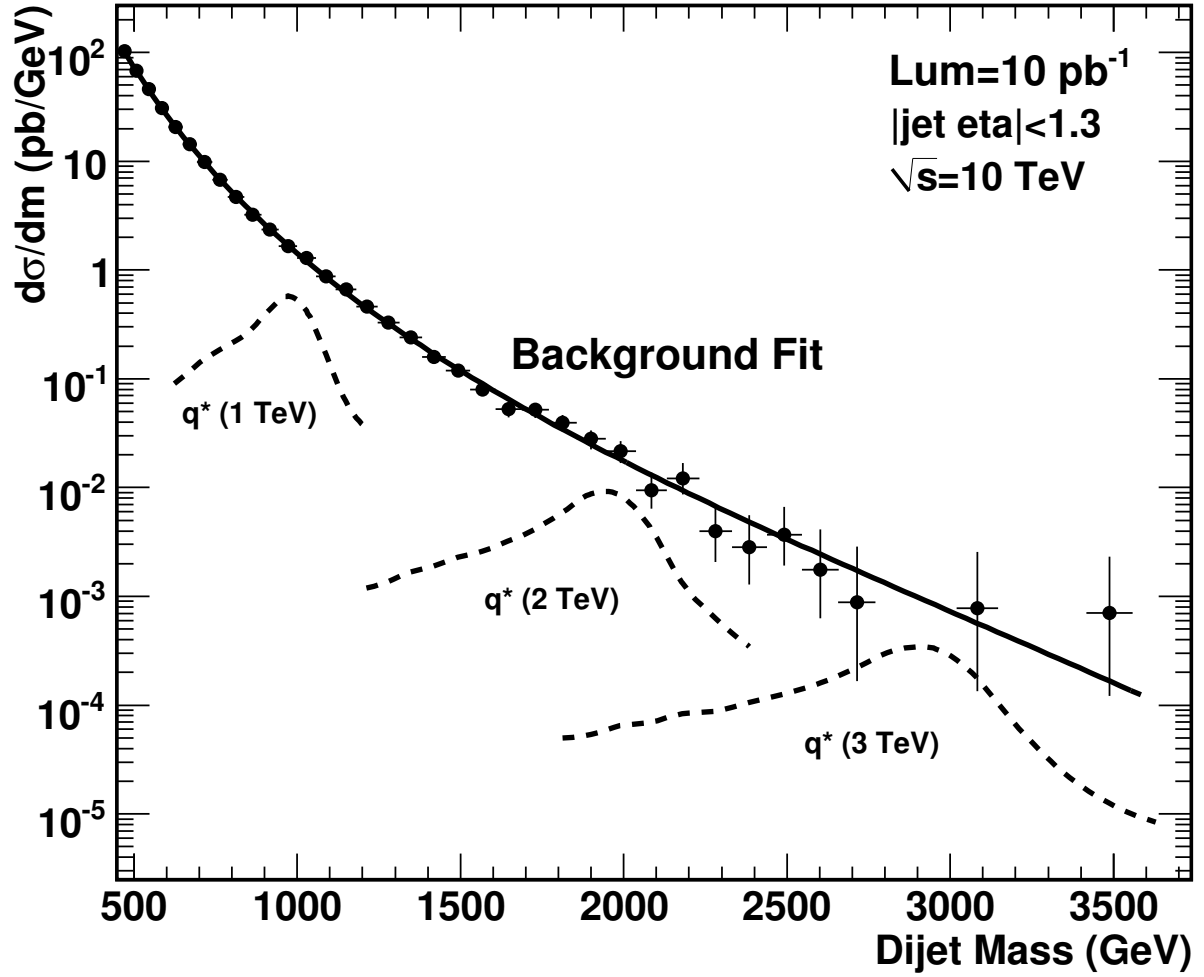
Figure 2: The dijet mass distribution (points) compared to a smooth background fit (solid curve) and to a simulation of excited quarks signals in the CMS detector (dashed curves). WARNING: CMS DATA IN THIS FIGURE IS FAKE
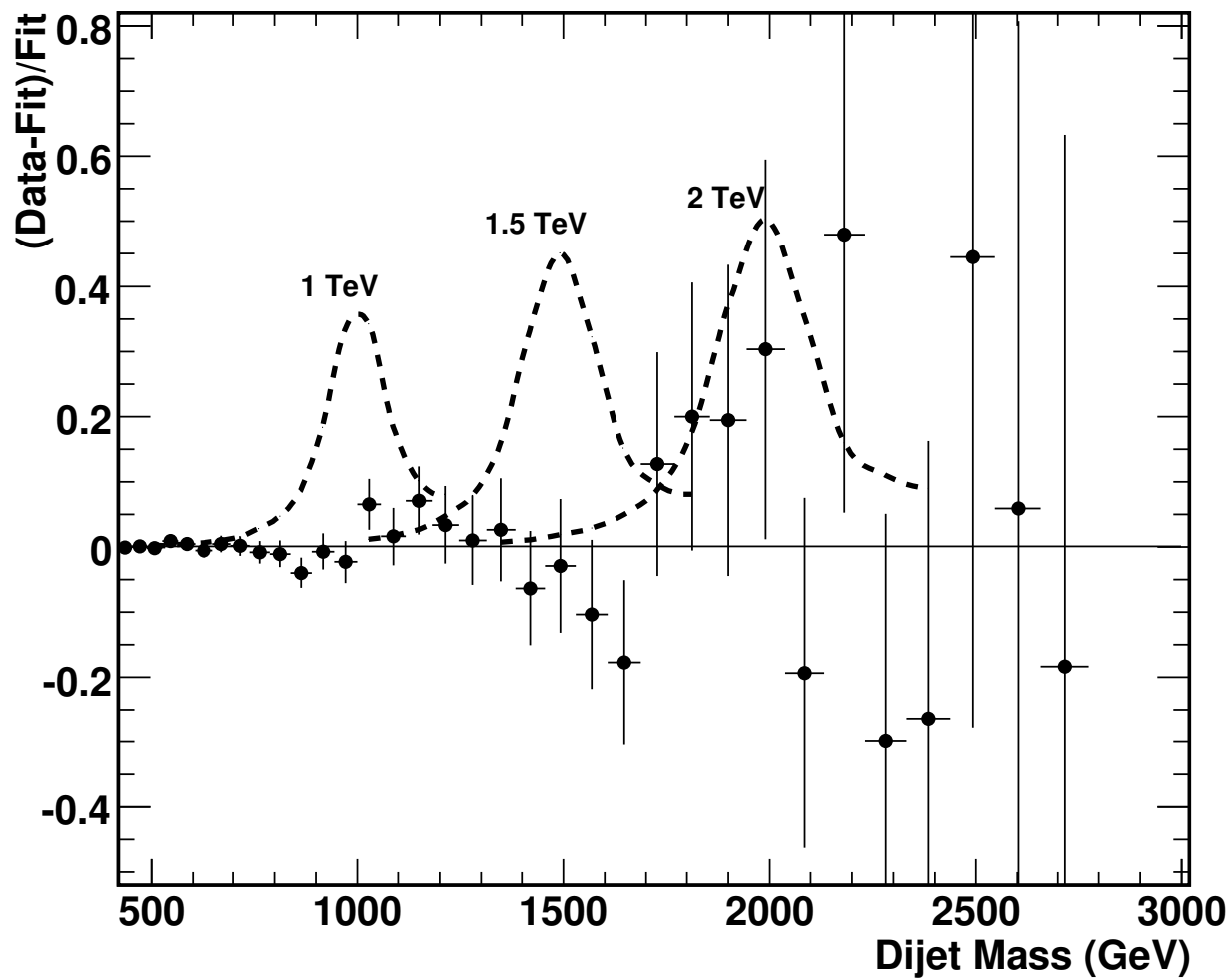
Figure 3: The fractional difference between the dijet mass distribution (points) and a smooth background fit (solid line) is compared to simulations of excited quark signals in the CMS detector (dashed curves). WARNING: CMS DATA IN THIS FIGURE IS FAKE
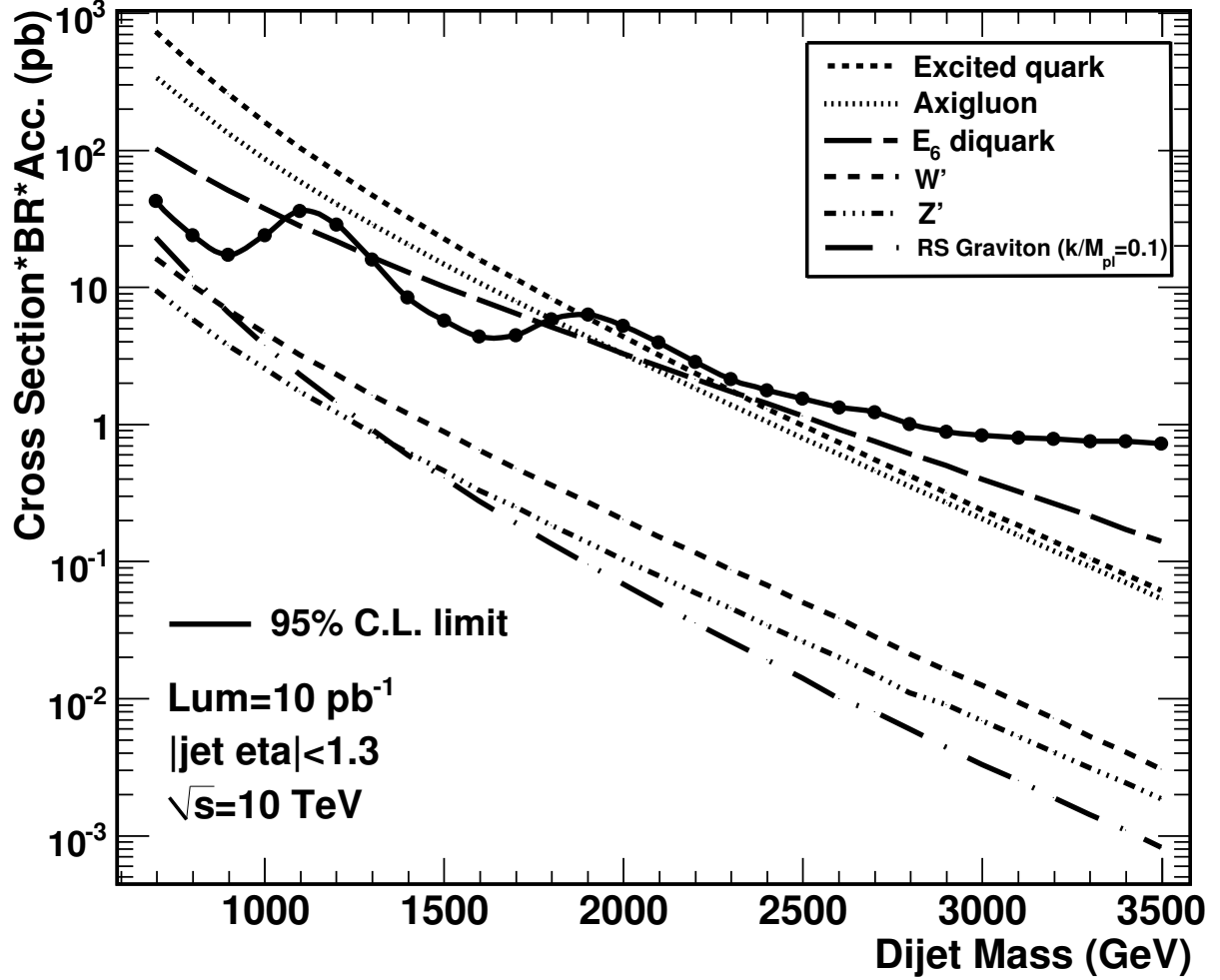
Figure 4: The upper limit on the cross section times branching ratio for new particles decaying to dijets (points) is compared to theoretical predictions for axigluons [1], flavor universal colorons [2], excited quarks [3], E_6 diquarks [4], Randall-Sundrum gravitons [6], and new gauge bosons W' and Z' [7]. The limit and theory curves require that both jets have pseudorapidity $|\eta| < 1.3$. WARNING: FROM FAKE DATA AND INCLUDING STATISTICAL UNCERTAINTIES ONLY

Mass (TeV/c^2)	95% C.L. $\sigma \cdot B$ (pb)	Mass (TeV/c^2)	95% C.L. $\sigma \cdot B$ (pb)
0.7	42	2.2	2.8
0.8	24	2.3	2.1
0.9	17	2.4	1.8
1.0	24	2.5	1.5
1.1	35	2.6	1.3
1.2	29	2.7	1.2
1.3	16	2.8	1.0
1.4	8.3	2.9	0.88
1.5	5.7	3.0	0.83
1.6	4.3	3.1	0.80
1.7	4.5	3.2	0.79
1.8	5.8	3.3	0.78
1.9	6.3	3.4	0.76
2.0	5.3	3.5	0.73
2.1	3.9		

Table I: As a function of new particle mass we list our 95% C.L. upper limit on cross section times branching ratio for narrow resonances decaying to dijets. The limit applies to the kinematic range where both jets have pseudorapidity $|\eta| < 1.3$ WARNING: FROM FAKE DATA AND INCLUDING STATISTICAL UNCERTAINTIES ONLY.